PAPER

Check for updates

Polyvinyl alcohol/propylene glycol facilitates reversible thermochromism of passive energy-saving flexible wood films at low (brightness) to high (depth) temperatures†

Zhe Kang, Nianrong Feng, Baorui Liu and Dongying Hu [iD] *

Reversible thermochromism presents depth at low temperatures and brightness at high temperatures, which is not conducive to the application of the passive energy-saving and shading effect. Here, we propose an innovative strategy for unconventional reversible thermochromic energy-storage flexible wood films (FT-PCMs-2) by the contribution of polyvinyl alcohol/propylene glycol (PVA/PG). Upon heating, the FT-PCMs-2 changes from light red/green to dark red/green, in contrast to the color change of the non-flexible composites without PVA/PG. The FT-PCMs-2 has good flexibility, mechanical strength and thermal stability. Among them, MSR-DEW-6PVA and MSG-DEW-6PVA have better comprehensive properties, including suitable phase change temperatures (38.6 °C and 37.2 °C), high latent heat values (59.79 J g^{-1} and 73.02 J g^{-1}), and low supercooling degrees (2 °C and 0.6 °C). FTIR, XRD and SEM analysis show that the binary fatty acid eutectics were successfully loaded into the eucalyptus fibre skeleton with physical interaction with PVA/PG. In addition, MSR-DEW-6PVA and MSG-DEW-6PVA have photothermal conversion rates of 48.3% and 36%, good cycling stability and anti-leakage performance after 50 cycles, and have promising applications in the fields of building energy saving, intelligent windows and decoration.

1 Introduction

Reducing the high building energy consumption caused by rapid urbanization and population growth is the primary task of building energy conservation. Transferring part of the peak load to off-peak hours is a promising passive energy saving initiative, depending on the thermal balance properties of building materials.[1,2] The use of phase-change energy storage materials (PCMs) in buildings is an effective way to passively cool and store heat energy without consuming electricity or fuel, easing reliance on fossil fuels.[3] By storing incident solar radiation, PCMs can lower the indoor temperature by 6–8 °C in summer and reduce the cooling load of the building. In winter, it can play a role of heat accumulator and raise the indoor temperature by 6–10 °C, so as to relieve the heat load of the building.[4]

Organic solid–liquid PCMs with suitable phase transition temperatures and high latent heats are the optimal choice for passive energy-saving applications in buildings.[5,6] Solving the

State Key Laboratory of Featured Metal Materials and Life-Cycle Safety for Composite Structures, MOE Key Laboratory of New Processing Technology for Nonferrous Metals and Materials, and School of Resources, Environment and Materials, Guangxi University, Nanning 530004, China. E-mail: hdygxu@163.com; 3526876264@qq. com; 1753615250@qq.com; 785631176@qq.com

problem of solid–liquid modified leakage is still the key to achieve shape stability. So, porous materials are often used as anti-seepage support materials, such as porous cellulose acetate film,[7] modified porous wood powder,[8] porous carbon,[9] graphite foam,[10] cotton-derived carbon sponge,[11] oriented carbon fiber,[12] silica,[13] hydroxyapatite[14] and perlite.[15] Wood has a good natural 3D layered anisotropic porous structure, which is used to prepare various wood-based phase change composites in combination with PCMs.[16–19] However, since traditional wood-based PCMs composites are solid and rigid when the temperature is lower than the phase change temperature, they are prone to brittle fracture under the action of external forces. And it is difficult to combine with other acting elements, which limits the application in fields requiring high flexibility.[20] With the development needs of flexible electronic devices, wearable devices and smart homes, flexible PCMs with excellent mechanical properties have become a research hotspot.[21–26]

Reversible thermochromic materials label surface temperature changes and temperature distribution through color memory, and are generally composed of couplers, developers, and co-solvents (fatty alcohols, fatty acids, *etc*).[27–29] PCMs can not only contribute to phase change energy storage, but also participate in thermochromic processes as co-solvents. The low thermal efficiency of visible light leads to a lot of waste in the process of solar radiation utilization. Photothermal conversion

is a key means to improve the efficiency of solar energy utilization. The organic combination of thermochromic (photothermal generation) and phase change energy storage may be a potential solution. We expect the composite PCMs formed by the integration of thermochromic components and phase change energy storage components to improve the absorption of visible light through thermochromism. Thereby to enhance solar thermal conversion and thermal energy storage, it effectively improves the solar thermal conversion efficiency and provides good visual experience though reversible thermochromic.

However, the reversible thermochromic phase change energy storage systems currently mainly researched often show the process of dark color formation at low temperature and light color decolorization at high temperature. It is not conducive to improving the absorption of light by composite materials through the dark effect. On the basis of the good stability and heat storage capacity of PCMs, how to realize the transformation for thermochromic properties of low temperature color depth-high temperature color lightness to low temperature color lightness-high temperature color depth, and build excellent composite PCMs with flexible and thermochromic properties is important. It uses thermochromic properties to improve the absorption of visible light to regulate the ambient temperature through solar energy storage-release passive energy saving and reduce power consumption. Undoubtedly, it opens a new door for its application in building energy saving, flexible devices, decoration and other fields.

This work takes full advantage of the dual identity of the organic binary fatty acid eutectic as co-solvents for both passive energy saving and reversible thermochromic complexes. The delignified eucalyptus fiber skeleton is used as passive energy-saving anti-leakage load support material, pressure impregnation and secondary compression are used to improve the bonding between components. And more, polyvinyl alcohol/propylene glycol are used as the key component of flexibility and surface encapsulation on flexible composites with dibasic fatty acid/eucalyptus wood fiber skeleton for passive energy saving contributed to the response of reversible unconventional thermotropic effects.

2 Experimental sections

2.1 Materials and reagents

Eucalyptus wood chips (60 mm × 60 mm × 1.5 mm) were purchased from a local wood product manufacturing and processing factory (Guangxi, China). Sodium hydroxide (NaOH) and sodium silicate (Na_2SiO_3) were provided by Sinopharm Chemical Reagent Co., Ltd (Shanghai, China). Magnesium sulfate ($MgSO_4$) and hydrogen peroxide (H_2O_2) were provided by Macklin Chemical Reagent Co., Ltd (Shanghai, China). 3, 3′-Bis(1-*n*-octyl-2-methylindol-3-yl)phthalide (BP, Red) and 2′-(dibenzylamino)-6′-(diethylamino)spiro [isobenzofuran-1(3H),9′-[9H]xanthene]-3-one (SO, Green) were purchased from Wuhan Haishan Technology Co., Ltd. Myristic acid (MA, $C_{14}H_{28}O_2$), palmitic acid (PA, $C_{16}H_{32}O_2$), stearic acid (SA, $C_{18}H_{36}O_2$), bisphenol A (BPA), diethylenetriaminepentaaceticacid (DTPA, $C_{14}H_{23}N_3O_{10}$),

propylene glycol (PG), and polyvinyl alcohol (PVA) were purchased from Shanghai Aladdin Biochemical Technology Co., Ltd (Shanghai, China).

2.2 Fabrication of reversible flexibility and thermochromic passive energy-saving flexible wood films

Firstly, the delignified eucalyptus fiber skeletons (DEWs) with a thickness of about 1.0 mm were prepared by the same methods reported in our previous paper (detailed in the supported materials).[30] Secondly, three binary fatty acid eutectic PCMs (FE: MA-PA, MA-SA, PA-SA) were selected and mixed with BP/SO, bisphenol A and binary fatty acids in the ratio of 1 : 1 : 50, melted at 75 °C and stirred thoroughly for 30 min to produce a red/green reversible thermochromic complex (FEC: MPR, MSR, PSR, MPG, MSG, PSG), referring to our previous work.[30] The molten red/green reversible thermochromic complex was injected into the 3D network fiber skeleton of DEWs by pressure immersion at 75 °C for 24 h, and the excess complex on the surface of the sample was removed with filter paper, dried at 75 °C for 24 h to obtain the binary eutectic fatty acid-based reversible thermochromic (low temperature dark color-high temperature light color) phase change energy storage materials (FT-PCMs: MPR-DEW, MSR-DEW, PSR-DEW, MPG-DEW, MSG-DEW, PSG-DEW).

Thirdly, FT-PCMs (60 mm × 60 mm) were hot pressed by different pressures with 40 N, 60 N, 80 N for 1 h was adopted to build thinner, leak-resistant, and more shape-stable FT-PCMs-1, named MPR-DEW-4, MPR-DEW-6, MPR-DEW-8. Other samples were named using the same strategy. After that, in order to make the above-obtained FT-PCMs-1 realize the transformation from the thermochromic properties of low temperature color depth-high temperature color lightness to low temperature color lightness-high temperature color depth, and achieve the purpose of complete encapsulation without leakage. The PVA/PG solution (PVA : PG = 1 wt% : 1 wt%) was prepared by adding PG to the 15 wt% PVA solution and stirred at 90 °C for 2 h as the encapsulation film-forming solution. FT-PCMs-1 were dipped into PVA/PG solutions for the pressure immersion in a vacuum drying oven at 75 °C for 2 h, taken out, and dried at 25 °C for 48 h to obtain the flexibility of FT-PCMs-2 (low temperature color lightness-high temperature color depth), named as MPR-DEW-4PVA, MPR-DEW-6PVA, MPR-DEW-8PVA. Other samples were named using the same strategy.

2.3 Characterization

The phase change characteristics of the samples (10 mg) were characterized using a differential scanning calorimeter (Netzsch, Shanghai, China) in the temperature range of −10 °C to 80 °C with 10 °C min^{-1}. Using an automatic colorimeter (ADCI-60-C, Chentaike, Beijing, China) to detect the color difference of the samples, including L, a, b, and other parameters. The chemical structures were measured using a Fourier transform infrared spectrometer (Nicolet iS 50, Thermo Fisher Co., Ltd. USA) within the testing range of 4000–500 cm^{-1}. The crystal structure were determined by using a DX-2700A X-ray diffractometer (Dandong Haoyuan Instrument Co., Ltd.

China) with the radiation tube pressure of 40 kV, the tube current of 30 mA, the scanning range of 5 to 65°, and the scanning rate of 10° min⁻¹. The mechanical properties were measured using a mechanical test system (universal testing machine 8801, INSTRON, England) with a sample size of 10 mm wide at a speed of 1 mm min⁻¹. The surface and cross-section micromorphologies of the samples were characterized by using a high resolution field emission scanning electron microscope (SIGMA500, Zeiss, Germany).

The thermodynamic stabilities were tested through using a thermogravimetric analyzer (TGA-Q500, Netzsch Instruments Co., Ltd. Germany) with the test conditions that sample mass was 5 mg, the heating rate was set to 10 °C min⁻¹. The infrared thermal imaging images of the samples at different temperatures were measured by an infrared thermal imager (FLUK TIS65, Fluke electronic instrument company, China). A solar simulator was used as the light source to measure the light-heat energy conversion and storage of the samples, and a K-type contact thermocouple thermometer was used to record the temperature change of the samples during the radiation and deradiation process of the solar simulator. A hot-plate test was performed to monitor the thermal energy storage-release characteristics of samples.

3 Results and discussion

3.1 The design of passive energy-saving flexible wood films

The phase change properties (melting/crystallization onset temperatures: T_m, T_s, peak temperatures: T_p, and latent heat values) of the binary eutectic fatty acid (FE), thermochromic binary eutectic fatty acid complex (FEC), binary eutectic fatty acid-based reversible thermochromic (low temperature dark color-high temperature light color) wood fiber-based composites (FT-PCMs) are shown in Table S1,† and binary eutectic fatty acid-based reversible thermochromic (low temperature color lightness-high temperature color depth) wood fiber-based films (FT-PCMs-2) are shown in Tables S2 and S3.† Compared to FE and FEC, all FT-PCMs showed lower phase change temperatures and substantially lower latent heat values. It is mainly because that the addition of BP/SO and BPA to the binary fatty acids affected the crystallisation of the fatty acids. And, the cellulose backbone structure of delignified eucalyptus wood also hindered the crystallisation of phase change materials, thus preventing the transition of molecular chains from ordered to disordered during the phase transition. In addition, the partial loss of the phase change material upon heating the impregnated PVA results in a reduction in the latent heat values of FT-PCMs-2.

With the increase of pressure, the phase transition temperature of the FT-PCMs-2 (red) first decreased and then increased, and the latent heat value decreased. It is mainly because that the pressure destroyed part of the crystalline region of cellulose, resulting in a decrease in the energy required for the phase transition and a decrease in the phase transition temperature. Under greater pressure, the hydrogen bonds between the cellulose molecules become tighter, resulting in increased intermolecular force and higher temperature. Under pressure,

the contact surface area increases, and the PCM loses more in the heated state, resulting in a decrease in latent heat value with increasing pressure.

The phase transition temperature of MA-SA-based FT-PCMs (38.6–39.2 °C) is lower than that of MA-PA-based FT-PCMs (41.6–43 °C), mainly because that the phase transition temperature of SA itself is lower than that of PA, MSR has a lower phase transition temperature than MPR, and MSR-DEW has a lower phase transition temperature than MPR-DEW as well. The latent heat values of MA-PA-based FT-PCMs (42.59–65.94 J g⁻¹) were not significantly different from those of MA-SA-based FT-PCMs (48.1–66.99 J g⁻¹). The supercooling of MA-SA-based FT-PCMs (0.9–2.7 °C) was lower than that of MA-PA-based FT-PCMs (4–6 °C). In addition, the higher phase transition temperature range of PA-SA-based FT-PCMs was 50.1–52.4 °C, which was determined by the higher phase transition temperature of PA and SA capability. The latent heat values and the supercooling degrees range of PA-SA-based FT-PCMs were 49.82–52.28 J g⁻¹ and 4–6.8 °C, which was lower and higher than those of MA-PA-based FT-PCMs. So MA-SA based FT-PCMs-2 (red and green) are the better choices.

3.2 The transformation for thermochromic properties of wood films

Tables S4 and S5† show the color parameters (L, a, b and ΔE) of the samples before and after heating to 75 °C. For the red FT-PCMs-2, the L and ΔE values decreased, a and b values increased after heating, indicating a decrease in brightness and a color shift toward red when the samples are heated. For FT-PCMs-2 with MPR, MSR and PSR as phase change materials, the color difference first increases and then decreases with increasing pressure. The total color difference values in descending order are PSR-DEW-6PVA > MSR-DEW-6PVA > MSR-DEW-8PVA > PSR-DEW-4PVA > MSR-DEW-4PVA > MPR-DEW-6PVA > MPR-DEW-8PVA > MPR-DEW-4PVA > PSR-DEW-8PVA. Therefore, PSR-DEW-6PVA, MSR-DEW-6PVA, and MSR-DEW-8PVA are the better choices. For the green FT-PCMs-2, the L, a and ΔE values of all samples except MPR-6PVA decreased after heating, and the b-value of most samples increased. It indicates that the brightness of the samples decreased after heating, and the color of the samples shifted towards green. For FT-PCMs-2 where MPG is the phase change material, MPG-DEW-6PVA has an increased and smaller difference in ΔE values and a smaller color change, so it is not an option. For MSG and PSG-based FT-PCMs-2, the color difference increases and then decreases as the pressure increases, so MSG-DEW-4PVA, MSG-DEW-6PVA, PSG-DEW-4PVA, and PSG-DEW-8PVA are the better choices because that the more obvious differences in chromatic aberration. According to the analysis in Tables S1–S3,† MSR-DEW-4PVA, MSR-DEW-6PVA, MPG-DEW-4PVA and MSG-DEW-6PVA with higher enthalpy and lower supercooling are the better choices. According to the analysis in Tables S4 and S5,† PSR-DEW-6PVA, MSR-DEW-6PVA, MSR-DEW-8PVA, MSG-DEW-4PVA, MSG-DEW-6PVA, PSG-DEW-4PVA and PSG-DEW-8PVA with good discolouration properties are the better choices. Combining the above analysis, MSR-DEW-6PVA and

MSG-DEW-6PVA were selected as the best choices for subsequent experiments and analysis.

Interestingly, for all FT-PCMs-1, after heating, the color of the sample changed from dark to light, and a fading process occurred. On the contrary, after heating, the color of all FT-PCMs-2 changed from light to dark, the BP-containing phase change composites changed from light red to dark red, and the SO-containing phase change composites changed from light green to dark green. The transformation for smart-response thermochromic properties of FT-PCMs-1 (red, green) of low temperature color depth-high temperature color lightness to FT-PCMs-2 (red, green) of low temperature color lightness-high temperature color depth has been successfully achieved. The difference between the two is whether the FT-PCMs-1 has been pressure impregnated with PVA/PG, followed by drying and encapsulation. Therefore, PVA/PG plays a key role in causing the distinct and unconventional inversion of color in FT-PCMs-1 and FT-PCMs-2.

Fig. 1 shows the mechanism of flexibility and reversible thermochromic of FT-PCMs-2. The prepared FT-PCMs-2 is supported by eucalyptus fiber skeleton with intermolecular hydrogen bonds of cellulose interacting with fatty alcohol/fatty acid. For the FT-PCMs-2, the color of the samples changed from dark red/green to light red/green after impregnation with PVA/PG solution. It may be attributed to the ionization of fatty acids in water, where the ionized H^+ interacts with the open BP/SO carboxylate ion in the water, which induces a change to a closed lactone ring structure. For FPCMs, the phase change material melted and the color changed from light to dark, and BP/SO changed from the lactone ring form to the open carboxylate form through hydrogen bonding interactions with bisphenol after heating. After cooling, the phase change material crystallized resulting in a darker to lighter color, and the BP/SO changed from an open carboxylate state to a lactone ring structure.

3.3 Analysis of chemical composition, structural characteristics, and thermal stability

Fig. 2a–c shows the FTIR spectra of samples. For DEW, the characteristic absorption peaks are located at 3438 cm^{-1} (O–H
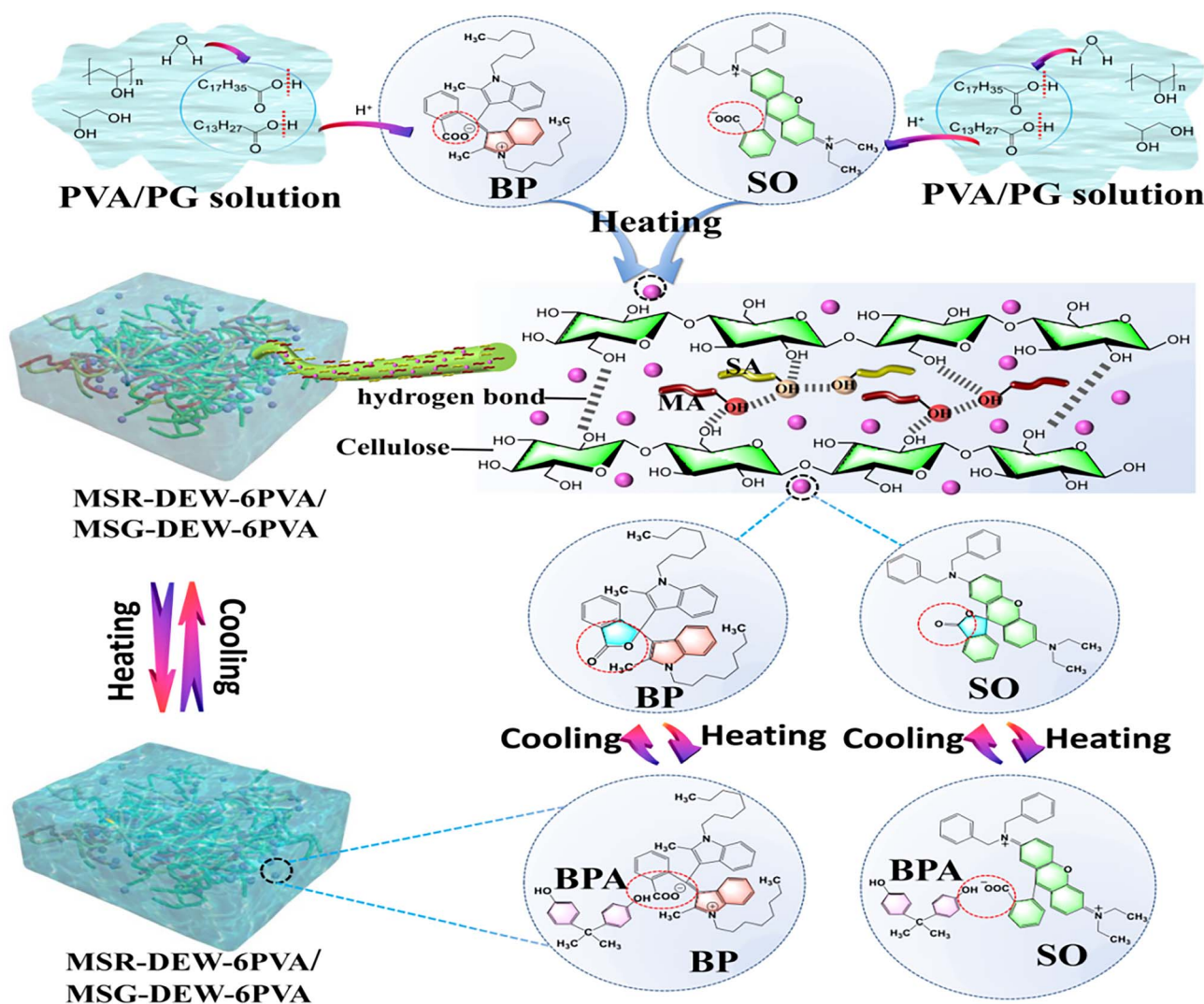

Fig. 1 Mechanisms of flexibility and reversible unconventional thermochromic of FT-PCMs-2.

stretching vibration), 2918 cm^{-1} and 2850 cm^{-1} (C–H stretching vibrations in methyl and methylene groups), 1637 cm^{-1} (benzene ring skeleton of lignin), 1464 cm^{-1} and 1403 cm^{-1} (–CH$_2$ deformation vibration). For PVA, the characteristic absorption peaks are located at 3458 cm^{-1} (O–H stretching vibration) and 1104 cm^{-1} (crystalline domains of PVA). Compared with DEW, the main characteristic peak of MSR-DEW-6 is weakened at 3434 cm^{-1} (the stretching vibration of –OH), enhanced at 2917 cm^{-1} and 2849 cm^{-1} (the C–H stretching vibration of –CH$_3$ and –CH$_2$), enhanced at 1467 cm^{-1} (the C–O in-plane bending vibration), and enhanced at 1057 cm^{-1} corresponding to the new peaks at 1707 cm^{-1} and 721 cm^{-1} (the C=O stretching vibration of MA-SA and the –CH$_2$ group), respectively. It indicates that MSR has been immersed in the internal structure of DEW, and there is a hydrogen bond interaction between the hydroxyl groups of MSR and DEW. After the addition of the PVA/PG mixture, the characteristic peak of MSR-DEW-6PVA was enhanced at 3429 cm^{-1}, mainly attributed to the strong –OH stretching vibrations of the PVA and PG

solutions. While the characteristic peaks of C–H stretching vibration corresponding to –CH$_3$ and –CH$_2$ were weakened at 2917 cm^{-1} and 2849 cm^{-1}, mainly attributed to partial leakage of MSR, and at 1704 cm^{-1} corresponds to the C=O stretching vibration of MA-SA, 1464 cm^{-1} to the C–O in-plane bending vibration, 1309 cm^{-1} to the C–O stretching vibration, 1038 cm^{-1} to the C–C stretching vibration and 719 cm^{-1} to the –CH$_2$ group of MA-SA. The characteristic absorption peaks of MSG-DEW-6 and MSG-DEW-6PVA are similar to those of MSR-DEW-6 and MSR-DEW-6PVA mentioned above. In addition, after the addition of the PVA/PG mixture, neither MSG-DEW-6PVA nor MSR-DEW-6PVA generated new characteristic peaks compared with MSG-DEW and MSR-DEW, indicating that there is no chemical reaction but only physical binding.

Fig. 2d shows the XRD patterns of samples. DEW shows two broad diffraction peaks at $2\theta = 15.94°$ and $22.64°$, which are classified as the 101 and 002 crystal planes of cellulose. The PVA shows diffraction peaks at $2\theta = 11.5, 19.5$ and $22.8°$, which are attributed to the 100, 101, and 200 diffraction planes of PVA,
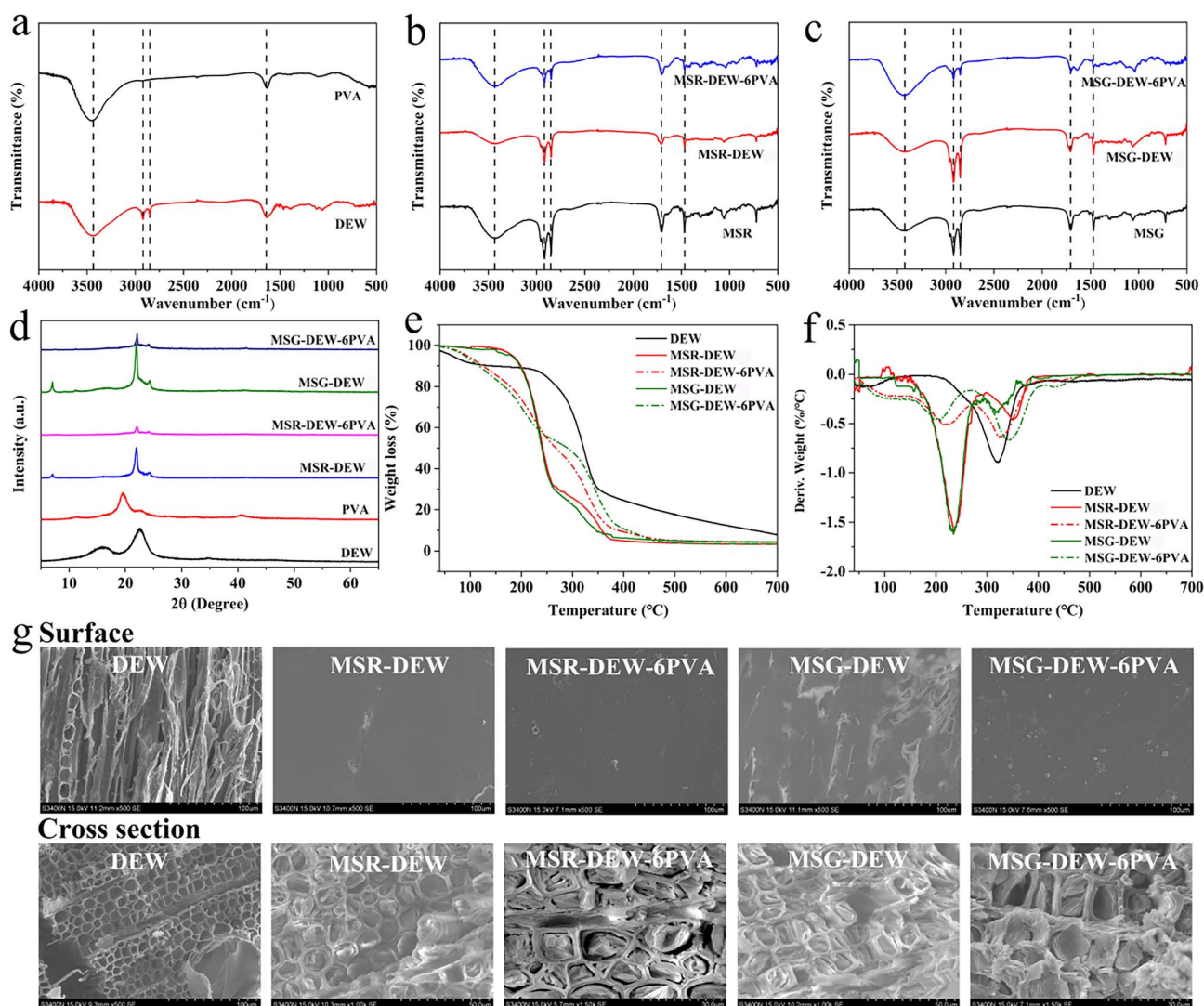

Fig. 2 FTIR spectra (a–c), XRD patterns (d), TGA-DTG (e and f) curves, and SEM images (g) of samples.

respectively.[31] For MSR-DEW-6, the main crystalline diffraction peaks are shown at $2\theta = 7.09°$, 22.03°, 24.36°. For MSR-DEW-6PVA, the main diffraction peaks are shown at $2\theta = 22.08°$ and 24.31°. These spikes are determined by the crystallographic indices of MA and SA, which indicate that MSR-DEW-6 and MSR-DEW-6PVA have a good crystal structure. In addition, compared with MSR-DEW-6, the intensity of XRD peaks of MSR-DEW-6PVA is weakened, indicating that the degree of crystallinity in the system is reduced, which also reflects the effect of PVA/PG on MSR-DEW-6. The change in the crystalline structure may also be the reason why MSR-DEW-6PVA exhibits the opposite thermochromic phenomenon compared to MSR-DEW-6, and the reason why MSR-DEW-6PVA has a thermally induced flexibility reversible transition. The same analysis results are also reflected in the XRD diffraction of MSG-DEW-6 and MSG-DEW-6PVA. Furthermore, neither the XRD patterns of FT-PCMs-1 nor FT-PCMs-2 formed new other diffraction peaks, confirming that the physical combination of FEC and DEW, and PVA/PG.

Fig. 2e and f shows the TGA-DTG curves of DEW, MSR-DEW-6, MSR-DEW-6PVA, MSG-DEW-6, and MSG-DEW-6PVA. For MSR-DEW-6, two distinct phases of weight loss were observed in the DTG curve. The maximum weight loss belonging to MA and SA is around 236 °C (162–280 °C), the weight loss belonging to BP, BPA and cellulose is around 349 °C (from 299–392 °C), the residual mass at 700 °C is 3.32%. For MSR-DEW-6PVA, the highest weight loss in the first stage is around 221 °C (155–270 °C), which belongs to MA and SA. And the highest weight loss in the second stage is 326 °C (278–396 °C), mainly due to the decomposition of BP, BPA, PVA and cellulose, with a residual mass of 4.4% at 700 °C. Compared with DEW, both MSR-DEW-6 and MSR-DEW-6PVA exhibited lower thermal degradation temperature, and lower residual mass at 700 °C. It implies the reduced thermal stability may be due to the addition of the red reversible thermochromic phase change complex (FEC: MSR). Furthermore, MSR-DEW-6PVA exhibited a higher residual mass at 700 °C compared with MSR-DEW-6, possibly due to the PVA/PG recombination. Similarly, the thermal stability analysis of MSG-DEW-6 and MSG-DEW-6PVA yielded the same results as the above-mentioned MSR-DEW-6 and MSR-DEW-6PVA.

Fig. 2g shows the SEM images of samples. The radial and interfacial structures of DEW exhibit a unique honeycomb-like porous structure, implying that it can be used as a good framework support for phase change materials. Compared with MSR-DEW and MSG-DEW, radial SEM micrographs of MSR-DEW-6PVA and MSG-DPW-6PVA show flat and smooth surface morphology. It means that the surface of MSR-DEW and MSG-DEW were covered with PVA/PG mixture. The cross-sectional view shows that the pore structure of DEW is filled with MSR and MSG, and the pore structure of MSR-DEW-6PVA and MSG-DPW-6PVA is crushed under pressure compared to MSR-DEW and MSG-DEW. In addition, the loading of MPG-DPW-6PVA is higher than that of MPR-DEW-6PVA, due to the smaller molecular weight of SO (Green) than BP (Red), which leads to easier immersion into the internal pore structure of DEW and tighter binding.

3.4 Polyvinyl alcohol/propylene glycol contributes to mechanical reinforcement and flexibility response

Fig. 3a is the mechanical diagram of samples. The addition of PVA significantly improved the mechanical properties of the samples. Fig. 3b, d and f shows the stress–strain curves of samples. The tensile strengths of DEW, MSR-DEW, MSR-DEW-6PVA, MSG-DEW and MSG-DEW-6PVA were 7.07 MPa, 20.40 MPa, 19.78 MPa, 18.69 MPa, and 24.18 MPa, respectively (Fig. 3c). The mechanical properties of the flexible samples were higher than those of the DEW, mainly due to the successful impregnation of the phase change material into the pore structure of DEW and the encapsulation of cellulose by PVA/PG. The mechanical strength of MSR-DEW-6PVA is lower than that of MSR-DEW, and that of MSG-DEW-6PVA is lower than that of MSG-DEW. It is probably due to the deformation of DEW caused by the pressure action, and the shrinkage and brittleness of PVA during dried processes, resulting in a decrease in mechanical strength. In addition, the structures of MSR-DEW and MSG-DEW were damaged due to the pressure, resulting in low mechanical strength of MSR-DEW and MSG-DEW, which could not be obtained by testing. The good mechanical properties of MSR-DEW-6PVA and MSG-DEW-6PVA also illustrate the mechanical enhancement of PVA/PG treatment.

Fig. 3e shows images of the flexibility of MSR-DEW-6PVA and MSG-DEW-6PVA. The anisotropy of DEW leads to anisotropic flexibility. MSR-DEW-6PVA and MSG-DEW-6PVA can be bent in any direction perpendicular to the wood fiber, with good curl flexibility, and good flexibility with no significant change after 100 bends. Fig. 3g reflects that MSG-DEW-6PVA is constantly repeated stretching under constant force and constant stretching speed. In the first 50 stretches, the general trend of strain gradually increases with the increase of the number of stretches. When the number of stretches is 200, the strain of MSG-DEW-6PVA reaches its maximum value. When the number of stretching is 200–350 times, the strain of the sample decreases very slowly with the increase of the number of stretching. When the number of stretching is greater than 350 times, the strain of the sample decreases obviously. Fig. 3h shows that MSR-DEW-6PVA is continuously and repeatedly stretched under constant force and constant stretching speed. In the first 50 stretches, with the increase of stretching times, the sample strain shows a certain fluctuation but the overall trend of strain keeps increasing. Fig. 3i is the loading diagram of samples with width of 5 mm. At first, all samples were able to withstand 200 g of weight without breaking. MSR-DEW and MSG-DEW could not bear 200 g weight for a long time and thus fracture occurred, while MSR-DEW-6PVA and MSG-DEW-6PVA could bear the 200 g weight for a long time. It indicates that the addition of PVA/PG greatly enhanced the toughness and mechanical strength of samples.

3.5 Photo-heat induced passive energy storage-release characteristics

Fig. 4a and b shows the DSC curves of samples. The endothermic range of MSR-DEW-6PVA ranges from 38.6 °C to 51.5 °C with 59.79 J g^{-1}, while that of MSG-DEW-6PVA ranges from
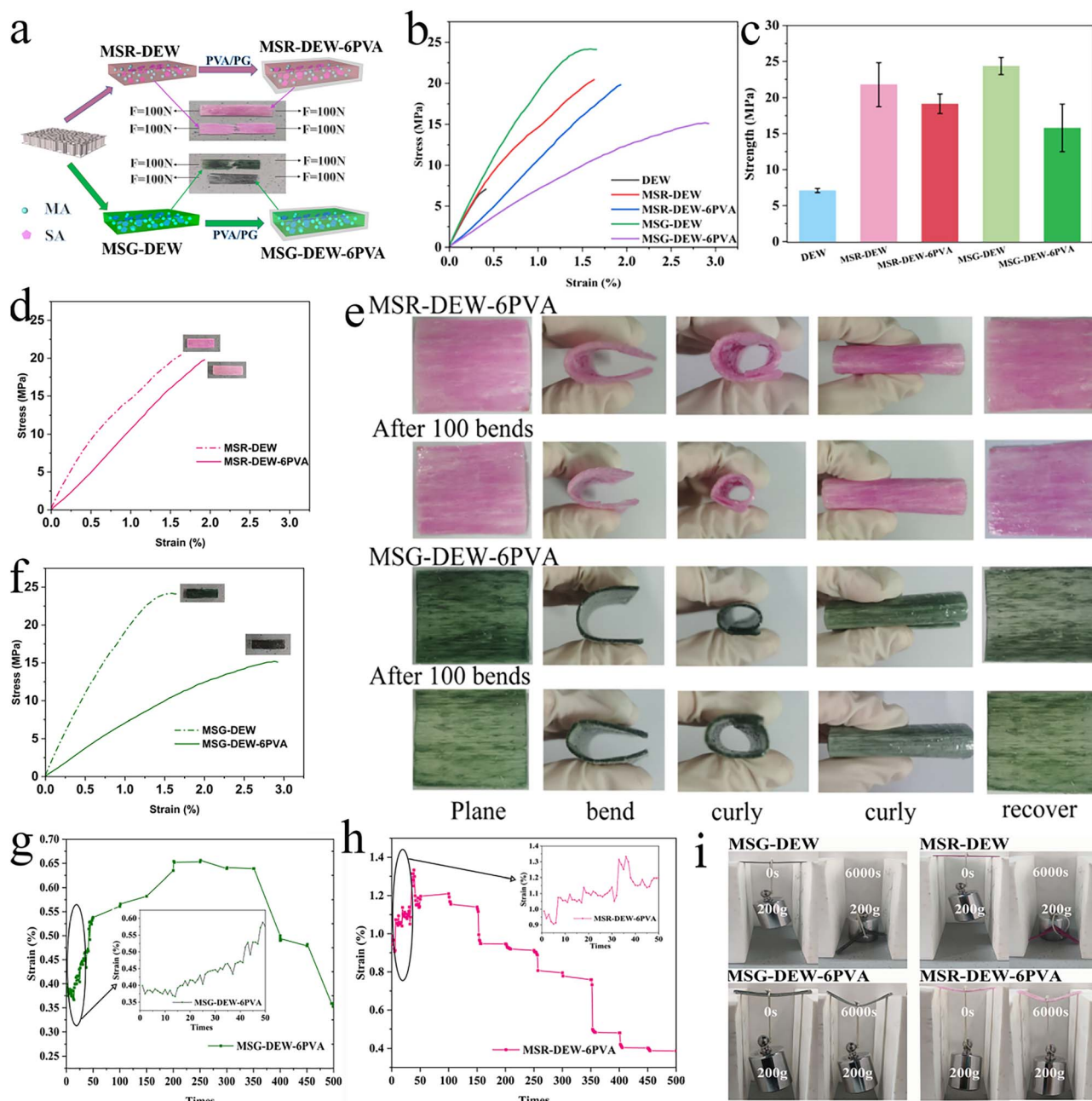
Fig. 3   Mechanical diagram (a), mechanical properties (b–d and f), flexibility images (e and i), mechanical durability (g and h) of samples.

36.6 °C to 47.4 °C with 73.02 J g⁻¹. MSR-DEW-6PVA and MSR-DEW-6PVA show better reversible energy storage effects than DEW, which is also confirmed by the analysis in Table S2.† The enthalpy values of MSG-DEW-6PVA at the endothermic stage (73.02 J g⁻¹) and exothermic stage (73.98 J g⁻¹) were higher than those of MSR-DEW-6PVA (59.79 J g⁻¹ and 69.05 J g⁻¹) (Fig. 4c), indicating the better phase-change energy storage of MSG-DEW-6PVA than that of MSG-DEW-6PVA.

Under solar radiation, the temperatures of MSR-DEW-6PVA and MSG-DEW-6PVA first increased rapidly, underwent a slow heat absorption stage, and then increased rapidly (Fig. 4d). MSR-DEW-6PVA and MSG-DEW-6PVA absorb light energy and convert it into heat to reach a maximum temperature of 70 °C in

51 s and 100 s, with a gentle heat absorption stage at 50.1–54 °C and 45.4–46 °C, corresponding to the solid–liquid phase transition stage. When the time was 500 s, the surface temperature of MSR-DEW-6PVA and MSG-DEW-6PVA dropped to 27.8 °C and 31 °C with a plateau at 39.3–38 °C and 37.7–36 °C, corresponding to the liquid–solid phase transition. MSR-DEW-6PVA and MSG-DEW-6PVA have good photo-thermal energy storage performance with photo-thermal conversion rates of 48.3% and 36%, respectively. Under the same cooling time, the temperature of MSR-DEW-6PVA and MSG-DEW-6PVA are higher than that of DEW, indicating the better passive energy storage-release characteristics.

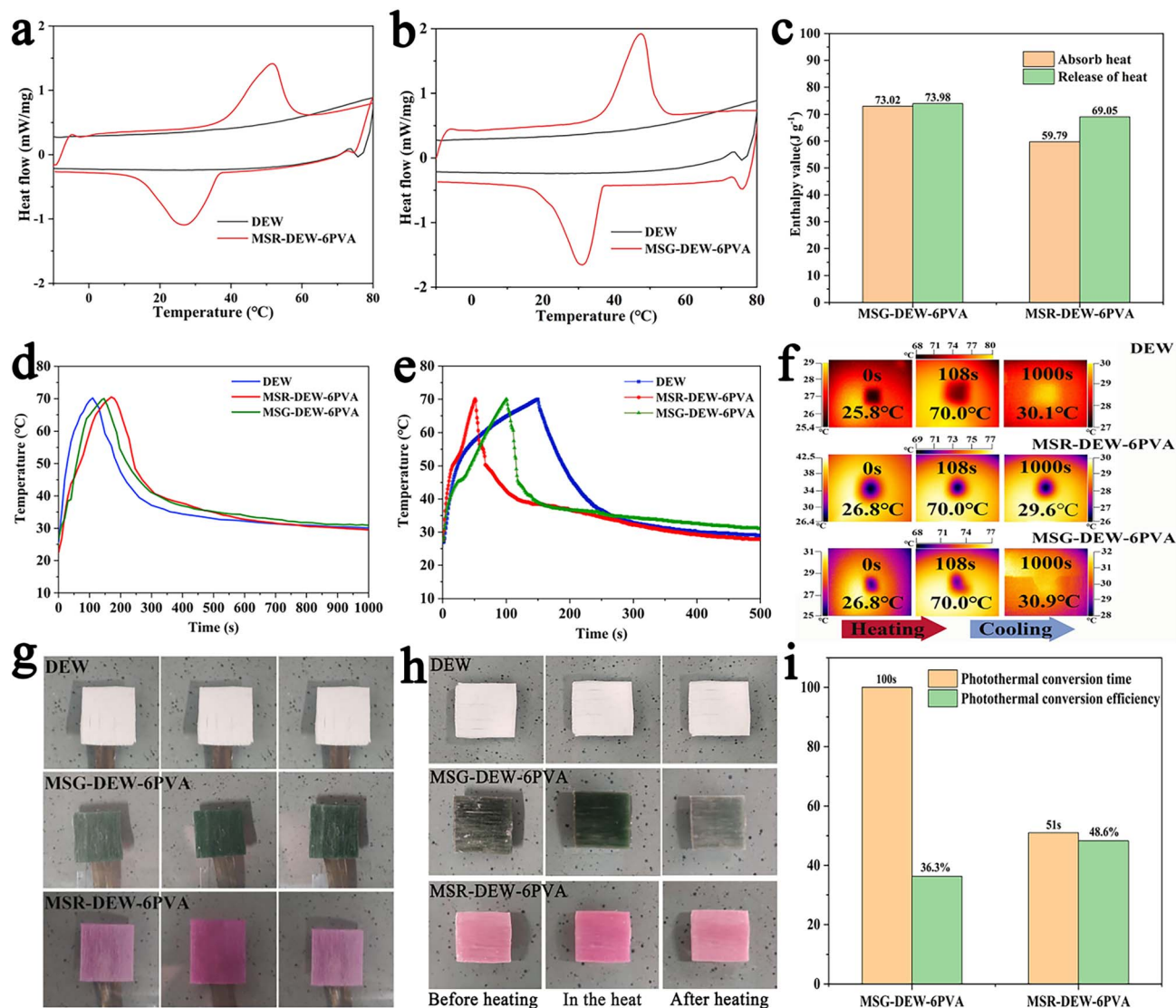The enthalpy values of MSG-DEW-6PVA at the endothermic stage

Fig. 4 DSC curves (a and b), heat absorption and heat release (c), the plots of temperature changes with time before and after sunlight (d), heating (e) processes, infrared thermographic images (f) during heating and cooling processes, sample images before and after light (g), sample images before and after heating (h), and photothermal conversion efficiency (i).

During heating, it takes 168 s for MSR-DEW-6PVA to rise from 26.8 °C to 70 °C, while it takes 145 s for MSG-DEW-6PVA to rise from 26.8 °C to 70 °C (Fig. 4e). It indicates that the heat transfer rate of MSR-DEW-6PVA is lower than that of MSG-DEW-6PVA, which is the opposite of the result of photothermal conversion. It may be due to the fact that the red object absorbs more light than the green object, as well as direct absorption of heat energy from the heating plate. MSR-DEW-6PVA has a relatively gentle heat absorption stage at 43.8–45.9 °C, and MSG-DEW-6PVA has a gentle heat absorption stage at 38.3–39 °C, which corresponds to the solid–liquid phase transition of the samples. During cooling, it took 832 s for MSR-DEW-6PVA to drop from 70 °C to 29.6 °C, with a gentle exothermic stage at 40.9–37.9 °C, and 855 s for MSG-DEW-6PVA to drop from 70 °C to 30.9 °C, with a gentle exothermic stage at 40.9–28.1 °C, corresponding to the liquid–solid phase change of the sample (Fig. 4f). MSG-DEW-6PVA has a higher holding capacity than

MSR-DEW-6PVA, which may be due to the higher latent heat value of MSG-DEW-6PVA loaded with more phase change material than MSR-DEW-6PVA, which is also consistent with the results of the thermal properties (DSC parameters) of FT-PCMs-2.

Fig. 4g and h shows the changes of samples before and after light and heating. The color of the sample is light before light, darkens during light, and returns to light after light. Compared with MSR-DEW-6PVA, MSR-DEW-6PVA has more obvious color changes before and after light, because dark green has stronger absorption and release ability of light than red. The color of the sample was light before heating, deepened during heating, and returned to light color after heating. Compared with MSR-DEW-6PVA, MSR-DEW-6PVA has more obvious color changes before and after heating. This may be that the effect of light causes red objects to absorb less light than green objects with a different wavelength range, which makes green materials have stronger

heat dissipating ability than red ones. It can also be seen that the sample has good uniformity and phase change energy storage performance.

Under strong light radiation, the sample temperature rose rapidly first, underwent a slow phase of heat absorption, and then rose rapidly. MSR-DEW-6PVA absorbed light energy and converted it into heat within 100 s, reaching the highest temperature of 70 °C, and its photothermal conversion efficiency was 59.9% (Fig. 4i). MSR-DEW-6PVA absorbed light energy and converted it into heat within 51 s. When the maximum temperature is 70 °C, the photothermal conversion efficiency is 77%. Both MSG-DEW-6PVA and MSG-DEW-6PVA have good photothermal energy storage performance.

3.6 Thermal cycling properties of passive energy-saving wood films

Fig. 5a and b shows the DSC curves of MSR-DEW-6PVA and MSG-DEW-6PVA before and after 50 heating–cooling cycles, verifying the passive energy conservation -encapsulation anti-leakage properties before and after thermal cycling of the samples. The enthalpy of MSR-DEW-6PVA-50cycles (heating: 64 J g^{-1}, cooling: 62.33 J g^{-1}) was lower than that of MSR-DEW-6PVA (heating: 59.79 J g^{-1}, cooling: 69.05 J g^{-1}) due to a small

amount of leakage during repeated heating–cooling cycles. The enthalpy of MSG-DEW-6PVA-50cycles (heating: 72.91 J g^{-1}, cooling: 74.73 J g^{-1}) differs very little from that of MSG-DEW-6PVA (heating: 73.02 J g^{-1}, cooling: 73.98 J g^{-1}), indicating that the sample is essentially no leakage, as can also be seen in the circulation photos.

After the heating–cooling cycle, the phase change temperatures of MSR-DEW-6PVA-50cycles and MSG-DEW-6PVA-50cycles were 38.4 °C and 34.7 °C, which was lower than the 38.6 °C of MSR-DEW-6PVA and 37.2 °C of MSG-DEW-6PVA, probably because the repeated heating–cooling cycle process leads to lower energy required for the phase change to occur. Furthermore, the supercooling of MSR-DEW-6PVA-50cycles (0.8 °C) was lower than that of MSR-DEW-6PVA (2 °C), while the supercooling of MSG-DEW-6PVA-50cycles (3.1 °C) was higher than that of MSG-DEW-6PVA (0.6 °C), probably due to the reduced crystallization capacity of the phase change material caused by repeated crystallization during the cycle.

Fig. 5c and d shows the weight loss of MSR-DEW-6PVA and MSG-DEW-6PVA with the increasing number of cycles. A certain degree of leakage occurs at first 5 cycles, and the leakage decreases with the increase of the number of cycles ranging from 5 to 30 cycles. This is mainly due to the fact that the initial
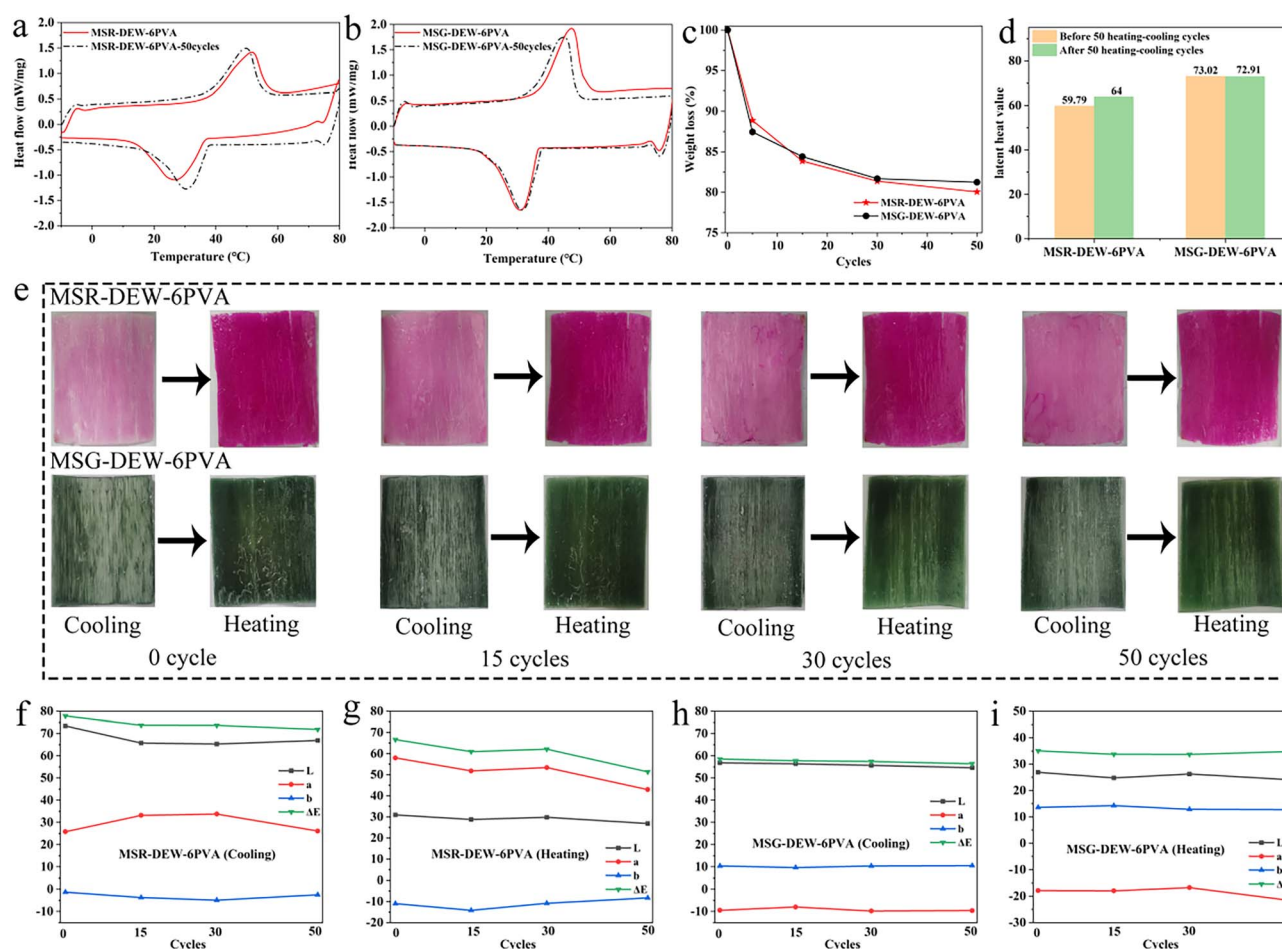

Fig. 5 DSC curves before and after 50 heating–cooling cycles (a and b), weight loss with increasing number of cycles (c), latent heat values (d), images at different cycles (e), color difference parameters at different cycle of MSR–DEW–6PVA (f and g) and MSG–DEW–6PVA (h and i).

surface of the sample loaded with a small amount of phase change material leaks during multiple heating and cooling cycles, and the sample has almost no leakage after 30 cycles, which also proves that it has good leakage resistance. Fig. 5d–i shows the latent heat values and photographs of MSR-DEW-6PVA and MSG-DEW-6PVA under multiple cycles with color difference parameters. After heating, the samples changed from light to dark, and the L, a, b and ΔE values did not differ significantly after multiple cycles. It also suggests that MSR-DEW-6PVA and MSG-DEW-6PVA have good thermal cycling stability in reversible thermochromic aspects.

4 Conclusion

In this work, a series of reversible flexibility and thermochromic passive energy-saving flexible wood films (FT-PCMs-2) were constructed by impregnating binary eutectic fatty acids/BP(SO)/bisphenol A into the DEW skeleton, then combined and pressed with the PVA/PG mixture. Comprehensive analysis shows that MSR-DEW-6PVA and MSG-DEW-6PVA had a good combined properties, including suitable phase change temperatures (38.6 °C and 37.2 °C), high latent heat values (59.79 J g^{-1} and 73.02 J g^{-1}) and low supercooling (2 °C and 0.6 °C). The binary fatty acid eutectic PCMs change from dark red/green to light red/green on heating, in contrast to the FPCMs which change from light red/green to dark red/green on heating. FTIR and XRD analysis showed that the bonding of the binary fatty acid eutectics with PVA/PG was only a physical interaction. SEM results show that the phase change material is successfully loaded into the eucalyptus fibre skeleton, and TG analysis shows that the FPCMs have good thermal stability below 100 °C. FT-PCMs-2 has good flexibility, can be bent and curled in a direction perpendicular to the wood fibre with little change after 100 repeated cycles. In addition, the photothermal conversions of MSR-DEW-6PVA and MSG-DEW-6PVA were 48.3% and 36%, respectively. Through 50 heating–cooling cycles, FT-PCMs-2 show good cycling stability and enhanced leakage resistance compared to CPCMs. It indicates that the addition of PVA/PG effectively improves the leakage problem of eutectic phase change materials.

Author contributions

Zhe Kang: writing–original draft. Nianrong Feng: conceptualization–investigation. Baorui Liu: methodology. Dongying Hu*: supervision, review and editing.

Conflicts of interest

No conflict of interest exits in the submission of this manuscript.

Acknowledgements

References

1 Y. Zhang, F. Wang, J. Duvigneau, Y. Wang, B. Wang, X. Feng, Z. Mao, G. J. Vancso and X. Sui, *ACS Sustain. Chem. Eng.*, 2021, **9**, 15442–15450.
2 C. Arumugam and S. Shaik, *Sustain. Energy Technol. Assess.*, 2021, **48**, 101657.
3 L. Chen, Y. Li and X. Lu, *IOP Conf. Ser.: Earth Environ. Sci.*, 2021, **638**, 012120.
4 S. Wijesuriya and P. C. Tabares-Velasco, *Appl. Therm. Eng.*, 2021, **188**, 116646.
5 Y. Gao, X. Zhang, X. Xu, L. Liu, Y. Zhao and S. Zhang, *J. Mol. Liq.*, 2021, **343**, 117554.
6 Y. Lin, Y. Jia, G. Alva and G. Fang, *Renewable Sustainable Energy Rev.*, 2018, **82**, 2730–2742.
7 J. Zhang, Y. Cai, X. Hou, C. Huang, H. Qiao and Q. Wei, *Fibers Polym.*, 2017, **18**, 253–263.
8 L. Ma, C. Guo, R. Ou, L. Sun, Q. Wang and L. Li, *Energy Fuels*, 2018, **32**, 5453–5461.
9 Y. Zhao, X. Min, Z. Huang, Y. g. Liu, X. Wu and M. Fang, *Energy Build.*, 2018, **158**, 1049–1062.
10 S. Duan, X. Wu, K. Zeng, T. Tao, Z. Huang, M. Fang, Y. Liu and X. Min, *Carbon*, 2020, **159**, 527–541.
11 N. Sheng, T. Nomura, C. Zhu, H. Habazaki and T. Akiyama, *Sol. Energy Mater. Sol. Cells*, 2019, **192**, 8–15.
12 N. Sheng, R. Zhu, K. Dong, T. Nomura, C. Zhu, Y. Aoki, H. Habazaki and T. Akiyama, *J. Mater. Chem. A*, 2019, **7**, 4934–4940.
13 Z. Fu, L. Dai, Y. Yi, J. Luo and B. Li, *J. Sol–Gel Sci. Technol.*, 2018, **87**, 419–426.
14 Y. Wang, D. Liang, F. Liu, W. Zhang, X. Di and C. Wang, *Appl. Therm. Eng.*, 2017, **113**, 1475–1482.
15 A. Karaipekli, A. Biçer, A. Sarı and V. V. Tyagi, *Energy Convers. Manage.*, 2017, **134**, 373–381.
16 H. Chen, J. Xuan, Q. Deng and Y. Gao, *Prog. Nat. Sci.: Mater. Int.*, 2022, **32**, 190–195.
17 H. Yang, W. Chao, X. Di, Z. Yang, T. Yang, Q. Yu, F. Liu, J. Li, G. Li and C. Wang, *Energy Convers. Manage.*, 2019, **200**, 112029.
18 H. Yang, Y. Wang, Q. Yu, G. Cao, R. Yang, J. Ke, X. Di, F. Liu, W. Zhang and C. Wang, *Appl. Energy*, 2018, **212**, 455–464.
19 A. Temiz, G. Hekimoğlu, G. Köse Demirel, A. Sarı and M. H. Mohamad Amini, *Int. J. Energy Res.*, 2020, **44**, 10495–10505.
20 X. Lin, S. Jia, J. Liu, X. Li, X. Guo and W. Sun, *J. Mater. Sci.*, 2021, **56**, 16570–16581.
21 H. Guan, J. Meng, Z. Cheng and X. Wang, *ACS Appl. Mater. Interfaces*, 2020, **12**, 46357–46365.
22 K. Takahashi, R. Ishii, T. Nakamura, A. Suzuki, T. Ebina, M. Yoshida, M. Kubota, T. T. Nge and T. Yamada, *Adv. Mater.*, 2017, **29**, 1606512.
23 Z. X. Wang, X. S. Han, Z. J. Zhou, W. Y. Meng, X. W. Han, S. J. Wang and J. W. Pu, *Compos. Sci. Technol.*, 2021, **213**, 108931.
24 C. Zhang, J. Mo, Q. Fu, Y. Liu, S. Wang and S. Nie, *Nano Energy*, 2021, **81**, 105637.

25 S. Lv, F. Fu, S. Wang, J. Huang and L. Hu, *RSC Adv.*, 2015, **5**, 2813–2818.

26 W. Zhang, B. Wang, J. Sun, Y. Li, J. Zhao, Y. Liu and H. Guo, *Adv. Mater. Interfaces*, 2022, **9**, 2101727.

27 N. Feng, Y. Liang and D. Hu, *J. Energy Storage*, 2020, **30**, 101401.

28 X. Geng, W. Li, Q. Yin, Y. Wang, N. Han, N. Wang, J. Bian, J. Wang and X. Zhang, *Energy*, 2018, **159**, 857–869.

29 O. Panák, M. Držková, M. Kaplanová, U. Novak and M. K. Gunde, *Dyes Pigm.*, 2017, **136**, 382–389.

30 N. Feng, Z. Kang and D. Hu, *Sol. Energy*, 2022, **236**, 522–532.

31 H. J. Kim, K. Charoensri, J. A. Ko and H. J. Park, *Prog. Org. Coat.*, 2022, **163**, 106634.